NANO LETTERS

pubs.acs.org/NanoLett

Letter

Electric-Field-Mediated In-Sensor Alignment of Antibody's Orientation to Enhance the Antibody−Antigen Binding for Ultrahigh Sensitivity Sensors

Hye Jin Kim, Dongsung Park, Yejin Park, Dae-Hyeong Kim, and Jinsik Kim*

Cite This: *Nano Lett.* 2022, 22, 6537−6544

Read Online

ACCESS | Metrics & More | Article Recommendations | Supporting Information

ABSTRACT: Applying an electric-field (*E*-field) during antibody immobilization aligns the orientation of the antibody on the biosensor surface, thereby enhancing the binding probability between the antibody and antigen and maximizing the sensitivity of the biosensor. In this study, a biosensor with enhanced antibody−antigen binding probability was developed using the alignment of polar antibodies (immunoglobulin G [IgG]) under an *E*-field applied inside the interdigitated electrodes. The optimal alignment condition was first theoretically calculated and then experimentally confirmed by comparing the impedance change before and after the alignment of IgG (a purified anti-β-amyloid antibody). With the optimized condition, the impedance change of the biosensor was maximized because of the alignment of IgG orientation on the sensor surface; the detection sensitivity of the antigen amyloid-beta 1−42 was also maximized. The *E*-field-based in-sensor alignment of antibodies is an easy and effective method for enhancing biosensor sensitivity.

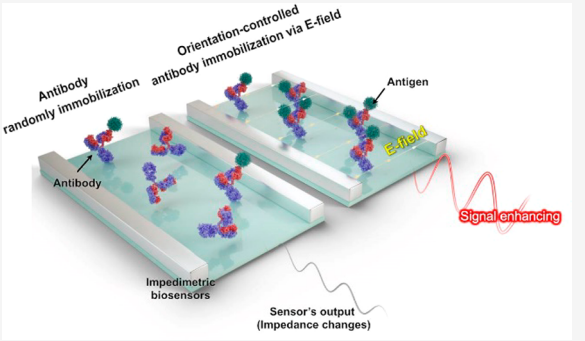

KEYWORDS: *antibody orientation, electric-field control, antibody−antigen binding, sensitivity, biosensor*

INTRODUCTION

Biosensing technology can be used to predict and diagnose diseases qualitatively or quantitatively based on complementary binding between biomarkers and receptors immobilized on the surface of the biosensor.[1−3] Therefore, biosensing technology must be highly sensitive and specific, and continuous development and optimization of both biomarkers and receptors is essential. For biomarkers, applying an electrostatic force, such as via electrophoresis[4] or dielectrophoresis,[5,6] can help derive higher concentrations of the target biomarkers in a biomatrix to establish highly sensitive and selective detection. Conversely, for the receptors, uniform immobilization, typically an antibody binding to a biomarker on the surface of the biosensor, can enhance sensor sensitivity and specificity by increasing the binding probability and biological activity between biomarker and antibody.[7]

Previous studies have used single-step immobilization methods, such as simple physical surface absorption and direct covalent immobilization, to uniformly immobilize the antibody to the biosensor surface.[8,9] Physical adsorption is the simplest method of immobilizing an antibody without any prerequisites for the type of antibody and surface modification;[10] however, it is limited by low stability, reproducibility, and controllability.[11,12] Meanwhile, direct covalent immobilization ensures high stability and controllability[13,14] but is sensitive to environmental factors, such as temperature[15] and humidity,[16] during the immobilization process and ionic concentration of the buffer.[17] Recently, multistep immobilization methods, including linker-mediated covalent and heterofunctional support techniques, have been utilized to immobilize antibodies.[18−23] In these multistep methods, the antibody is first adsorbed onto a substrate in a reversible manner and, then, is covalently linked using an appropriate linker;[24] hence, these methods allow for the control of the orientation of the antibody. As a result, the biological activity, and stability, and orientation of the antibody are improved. Unfortunately, however, because the multistep immobilization methods are also based on the reaction of specific biological substances and chemicals: (1) the available chemicals are limited by the binding site of the antibody open on the surface and (2) appropriate temperature and sufficient reaction time are required for antibody immobilization stability. In addition, because of the bulk-to-surface reaction process during multistep antibody immobilization and the natural abundance

Received: April 25, 2022
Revised: July 26, 2022
Published: July 28, 2022

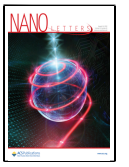

https://doi.org/10.1021/acs.nanolett.2c01584
Nano Lett. 2022, 22, 6537−6544

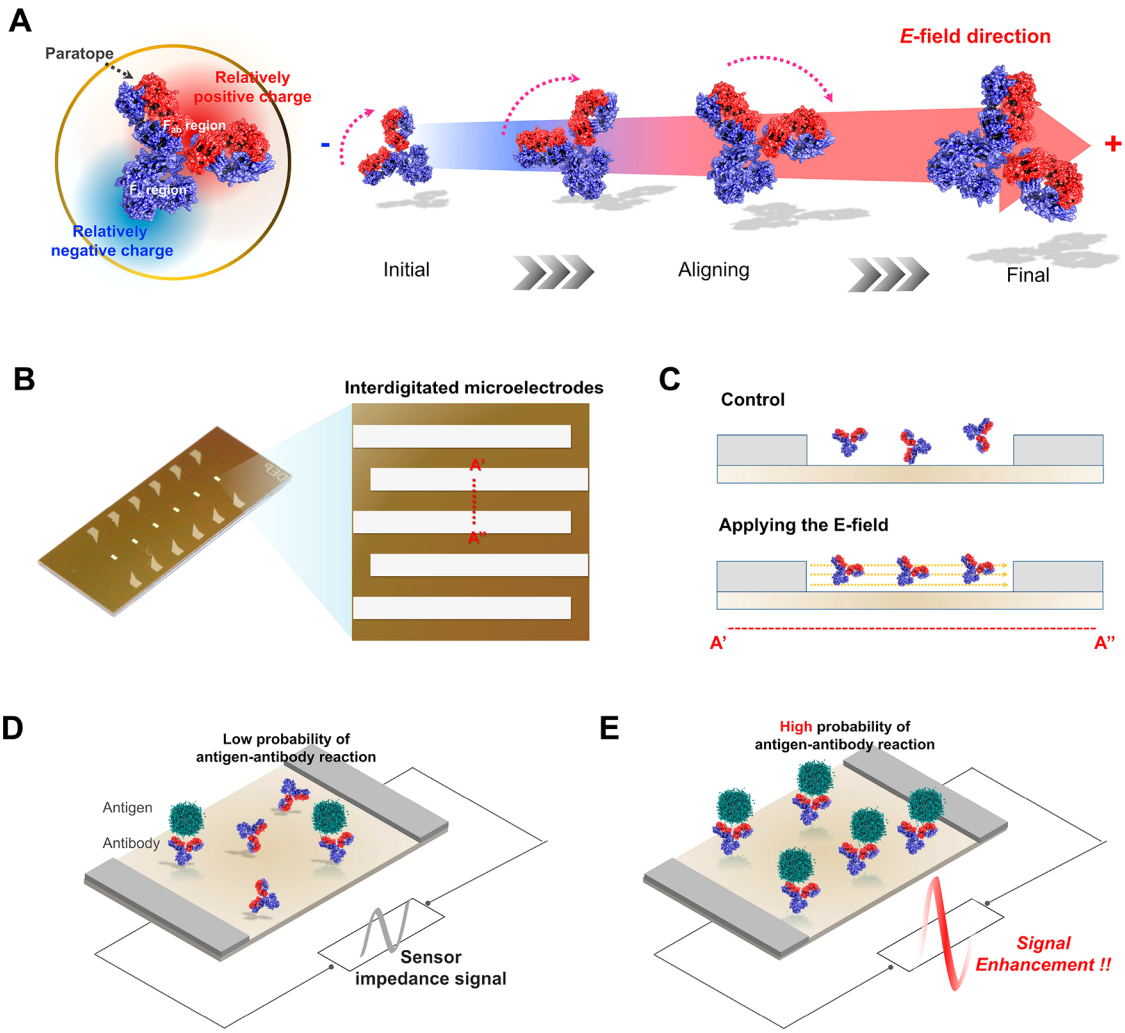

Figure 1. Aligning the orientation of antibodies via electric field (*E*-field) to enhance the antibody−antigen binding sensitivity. (A) The opposite charges of the F_{ab} and F_c regions of IgG cause IgG alignment according to the applied *E*-field. (B) A biosensor with interdigitated microelectrodes (IMEs) and (C) IgG immobilization process to align IgG orientation. (D, E) Uniformly immobilized IgG on the sensor surface enhances the biosensing signal.

of antibodies, chemical/biological multistep immobilization methods may be insufficient for complete antibody orientation control.[25,26]

Here, we developed a biosensor with an improved antibody−antigen binding probability using an electric-field (*E*-field)-based in-sensor alignment of the antibody ($A\beta_{42}$-specific immunoglobin G [IgG]) orientation (Figure 1). Using the developed biosensor, amyloid-beta 1−42 ($A\beta_{42}$), a major hall-marker of Alzheimer's disease (AD),[27,28] was detected with high sensitivity. As shown in Figure 1A, the opposite charge of the antigen binding (F_{ab}) and the fragment crystallizable region (F_c) of IgG resulted in dipole-like properties. A biosensor with interdigitated microelectrodes (IMEs) was fabricated (Figure 1B) and *E*-field was applied to the IMEs during the IgG immobilization on the biosensor surface (Figure 1C). In the control electrode to which no *E*-field was applied, the IgG was randomly immobilized on the surface between the IMEs, resulting in a small impedance change of the IMEs due to the weak IgG-antigen binding (Figure 1D). In contrast, in the IMEs to which *E*-field was applied, the probability of antigen-IgG binding was increased due to the alignment of the IgG orientation along the direction of *E*-field (i.e., the paratope at the edge of F_{ab} region of IgG was uniformly exposed outward) (Figure 1E). Consequently, the biosensor sensitivity in both phosphate-buffered saline (PBS) and standard plasma could be enhanced approximately 2.3-fold.

RESULTS AND DISCUSSION

Antibodies comprise a constant region with common amino acid sequences and a variable region with antibody-specific amino acid sequences that impart unique characteristics to the antibody.[29,30] In addition, antibodies exhibit an isoelectric point (pI value) because of the positively charged alkaline amino acids (arginine, lysine, histidine) and negatively charged acidic amino acids (glutamic and aspartic acids).[31,32] These charged amino acids are distributed in pairs of F_{ab} and F_c fragments, respectively.[33,34] Therefore, the fragments of an antibody exhibit charge heterogeneity that induces positive polarity for the F_{ab} fragments and negative polarity for the F_c fragments.[35−37] Such polarity allows for the migration, rotation, and vibration of an antibody to be controlled via the *E*-field,[38] further aligning the antibody along the direction of the applied *E*-field.[38−40] The angle (θ) of IgG, a

https://doi.org/10.1021/acs.nanolett.2c01584
Nano Lett. 2022, 22, 6537−6544

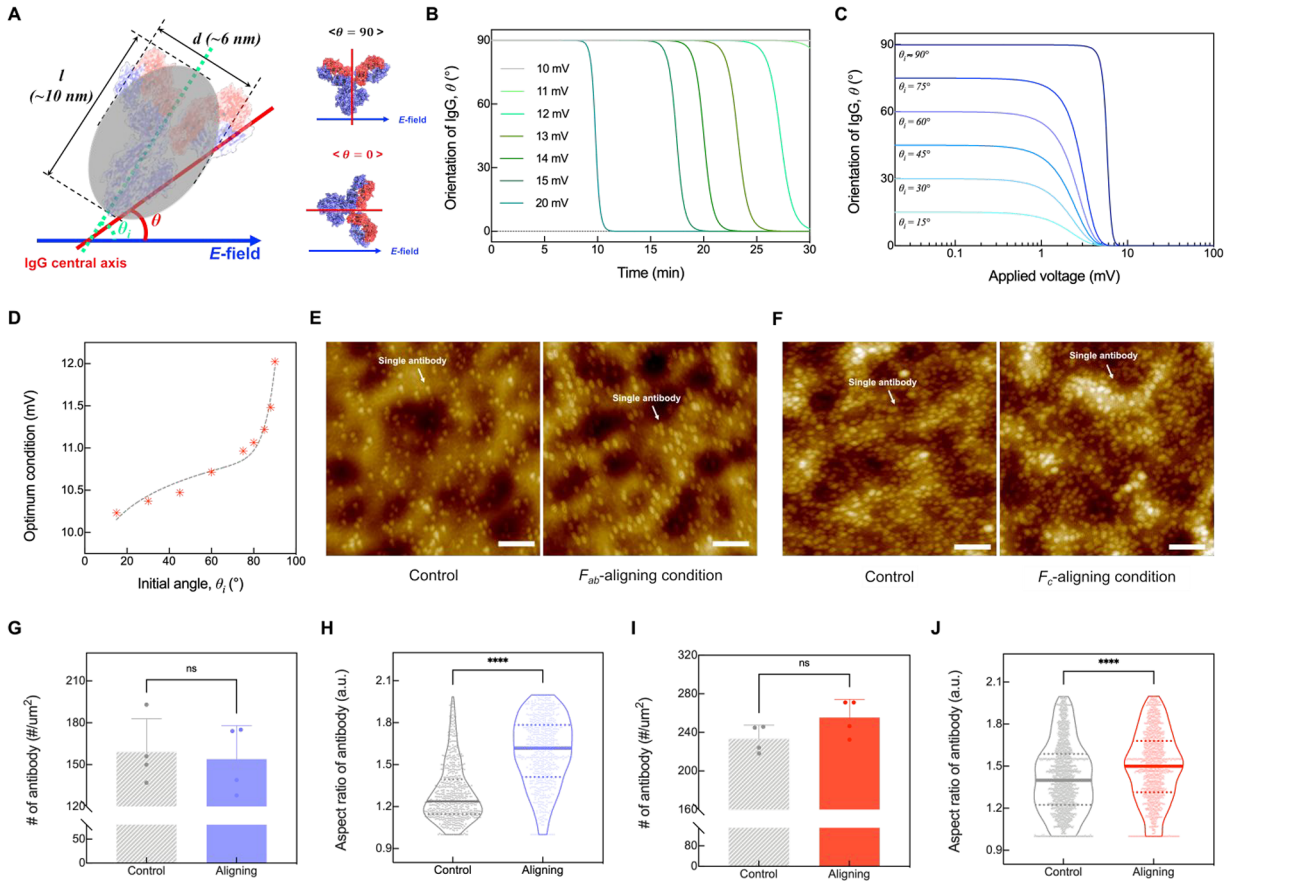

Figure 2. Aligning the IgG by an *E*-field. (A) Modeling of IgG. The angle of IgG (θ) relative to the direction of the *E*-field according to the (B) intensity of the applied voltage and (C) the initial angle (θ_i) of IgG. (D) The theoretical optimal condition required to align IgG parallel to the direction of the *E*-field according to the initial angle (θ_i) of IgG. The sensor surface observed after immobilizing the (E) F_{ab} and (F) F_c regions of IgG. The left and right images of (E) and (F) were acquired under the control and optimal aligning conditions, respectively. Scale bar = 0.5 μm. (G) Quantity of immobilized IgG on the sensor surface and (H) the aspect ratio of immobilized IgG in the optimal F_{ab}-aligning condition. (I) Quantification of immobilized IgG on the sensor surface and (J) aspect ratio of immobilized IgG in the optimal F_c-aligning condition.

representative type of antibody, relative to the *E*-field can change according to the intensity of the applied voltage and time (Figure 2A). The alignment of IgG under the applied *E*-field was studied both theoretically and experimentally. Initially, if no *E*-field is applied, the antibody randomly vibrates in the buffer because of the Brownian force. The random vibration is gradually suppressed as the *E*-field is applied, and when the random vibration of the antibody is completely suppressed, the antibody rotates along the direction of the *E*-field. At an applied voltage of 10 mV, IgG did not respond to the *E*-field, regardless of the duration. However, at ≥11 mV (placed perpendicular to the direction of the *E*-field (θ_i = 90°)), IgG rotated and eventually was aligned parallel to the direction of the *E*-field (θ = 0°). The results suggested that at least 11 mV is required for the IgG alignment (Figure 2B). Additionally, the intensity of voltage required for the IgG alignment was dependent on the initial angle of IgG (θ_i) relative to the *E*-field (Figure 2C).

The results showed that IgG rarely rotated before the intensity of the voltage reached approximately 1 mV, but the angle of IgG rotation gradually increased with the increase in voltage, and it eventually became parallel to the *E*-field at 10 mV. Herein, the voltage at which IgG and the *E*-field became parallel (θ = 0°) is defined as the optimal voltage condition; the corresponding voltages were plotted depending on the initial angle (Figure 2D). The results showed that the intensity of the optimal voltage increased linearly from 10.23 to 11.48 mV as the initial angle of IgG increased until it reached 90° (power series fitting: $y = a \cdot x^b + c \cdot x^d$, a = 9.11; b = 0.40; c = 1.11 × 10^{-36}; d = 18.41) and the voltage increased sharply to 17.78 mV at θ_i = 90°.

Rotation of IgG orientation was confirmed by observing the surface of the sensor using an atomic force microscope (AFM) (Figure 2E, F). The sensor surface was treated with high IgG concentration (1 ng mL^{-1} purified anti-β-amyloid antibody in 10 mM PBS, pH 7.4) under the optimal F_{ab}- and F_c-aligning conditions (30 and 20 mV, respectively). Herein, each optimal condition refers to a state in which the F_{ab} or F_c region of IgG is immobilized facing outward from the sensor surface (Figure S1); a detailed experiment to demonstrate the optimal conditions is described in the next section. The AFM image of the sensor surface was quantitatively analyzed through image processing (Figures S2 and S3). The surface of the bare substrate to which the antibody was not immobilized was also confirmed (Figure S4). The quantitative analysis revealed that the number of immobilized IgG on the sensor surface under F_{ab}-aligning condition (159.00 ± 10.40) was similar to that in the control (~159.00 ± 10.40; ~154.00 ± 10.43; p = ns, one-way analysis of variance [ANOVA]). However, the aspect ratio (AR) of the immobilized IgG on the sensor surface increased from ~1.30 ± 0.21 to ~1.59 ± 0.25 (p < 0.0001, one-way ANOVA) via *E*-field−based alignment (Figure 2G, H). Similar

https://doi.org/10.1021/acs.nanolett.2c01584
Nano Lett. 2022, 22, 6537−6544

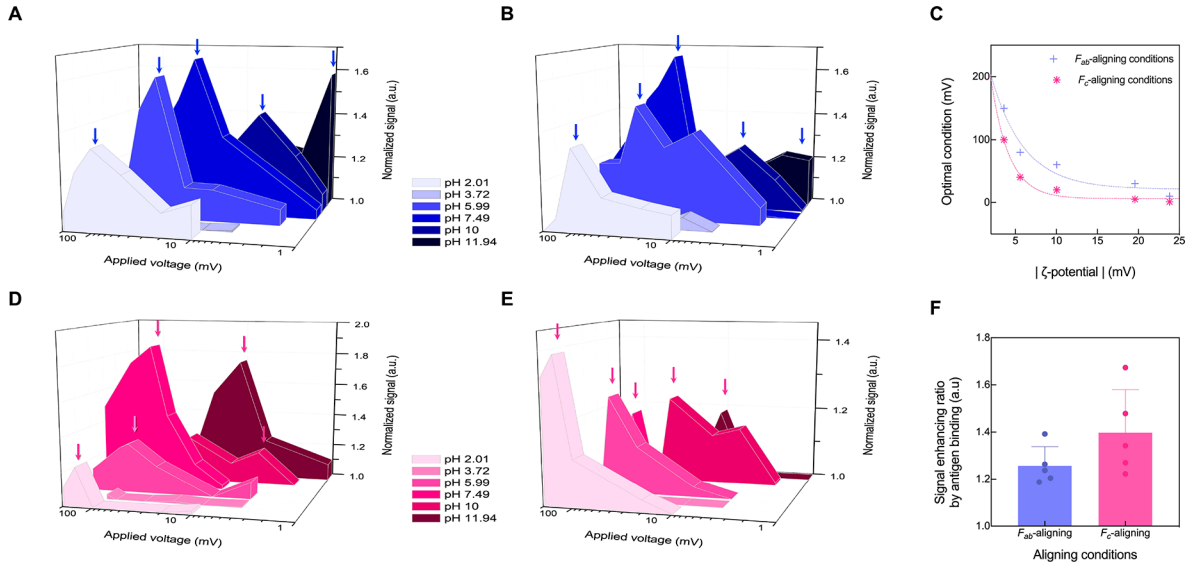

Figure 3. Changes in the impedance by immobilization of the (A) F_{ab} and (B) F_c regions of IgG. (C) Comparison of theoretical and experimental optimal voltages for aligning IgG according to its |ζ-potential|. Error bars represent the mean ± SD (n = 18). Changes in the impedance because of the antigen binding in the aligned (D) F_{ab}- and (E) F_c-region immobilized sensor. (F) Signal enhancing ratio of impedance change by antigen binding under each optimal aligning conditions.

to the F_{ab}-aligning results, even under the F_c-aligning condition, the difference in the number of IgG immobilized on the sensor surface was small (~238.78 ± 5.99; ~255.33 ± 8.27; p = ns, one-way ANOVA); however, the difference in AR values was significant (~1.42 ± 0.25; ~1.50 ± 0.25; $p < 0.0001$, one-way ANOVA) (Figure 2I, J). These results implied that improving the change in impedance under each alignment condition was not caused by the increased density of immobilized IgG on the sensor surface but rather by the aligning the orientation of the immobilized IgG.

The optimal aligning condition is influenced by the surface charge of IgG in addition to the initial angle of IgG and the intensity of the applied voltage. Thus, the effect of the surface charge of IgG (|ζ-potential|) on the IgG alignment was confirmed by measuring the impedance change occurred when IgG with different charges was immobilized on the surface of the sensor while applying various voltages. The |ζ-potential| of IgG was altered by controlling the pH of the buffer (pH 2.01−11.94) (Figure S5 and Table S1). Then, by binding the antigen ($A\beta_{42}$) to the orientation-controlled IgG, we verified that the binding probability of the antigen to IgG was changed by the antibody orientation.

The F_{ab} and F_c regions of IgG were immobilized on the sensor surface (Figure 3A, B). In the immobilization of IgG with ~3.59 ± 0.93 mV of |ζ-potential| in PBS (pH 2.01), a maximum change in impedance was observed at 150 and 100 mV by the immobilization of the F_{ab} and F_c regions, respectively. The impedance change was decreased as the applied voltage increased. The results indicated that the randomly oriented F_{ab} or F_c regions of the IgG aligned face outward from the sensor surface as the intensity of the applied voltage reached 150 and 100 mV, respectively. Then, when the applied voltage exceeded 150 mV and 100 mV, IgG migrated along the E-field, causing adsorption on the electrode surface. Therefore, the intensity of the applied voltage of the optimal F_{ab}- and F_c-aligning conditions was determined to be 150 and 100 mV, respectively, and the corresponding voltages were defined as respective optimal voltages. In addition, the optimal aligning conditions in PBS at various pH values (5.99, 7.49, 10.04, and 11.94) were confirmed.

Consequently, the optimal voltages were decreased exponentially along with the increasing |ζ-potential| of IgG (Figure 3C). However, in PBS at pH 3.72, the changes in impedance by IgG immobilization showed a random tendency depending on the applied voltage, because the surface charge of IgG at pH 3.72 was too small for the IgG to align with the E-field (|ζ-potential| = ~0.66 ± 0.21 mV) (Figure S6A); the values are presented in the Tables S2−S5. Furthermore, the changes in impedance due to immunoglobulin A (IgA) immobilization were measured according to the intensity of the E-field. Unlike IgG, the changes in impedance from IgA immobilization were unaffected by the E-field, which could be attributed to the difference in the structural conformation according to the isotypes (Figure S7).[24] These results suggest that aligning antibody orientation using an E-field is influenced not only by the strength of the charge held by the antibody but also by its structural conformation.

The alignment of IgG affects the binding probability of the antigen. The impedance changes according to antigen binding were varied according to the voltage applied during IgG immobilization (Figure 3D, E). Under each optimal IgG-aligning conditions, the maximum impedance change was observed, and enhancing ratios of impedance changes comparing the values measured in the control conditions were approximately 1.26 ± 0.07% and 1.40 ± 0.16% in the F_{ab}- and F_c-aligning conditions, respectively (Figure 3F). A higher enhancing value in the F_c-aligning conditions than that in the F_{ab}-aligning conditions suggests that the uniform alignment of the F_c region in IgG improved the probability of binding between the paratope and the epitope, thereby improving the binding affinity between IgG and the antigen.

The enhanced reaction probability between IgG and antigen was verified by counting the number of gold nanoparticles (AuNPs) after the binding of the AuNP-labeled secondary antibody to the antigen bound to the immobilized IgG. The number of AuNPs was calculated by averaging the value

https://doi.org/10.1021/acs.nanolett.2c01584
Nano Lett. 2022, 22, 6537−6544

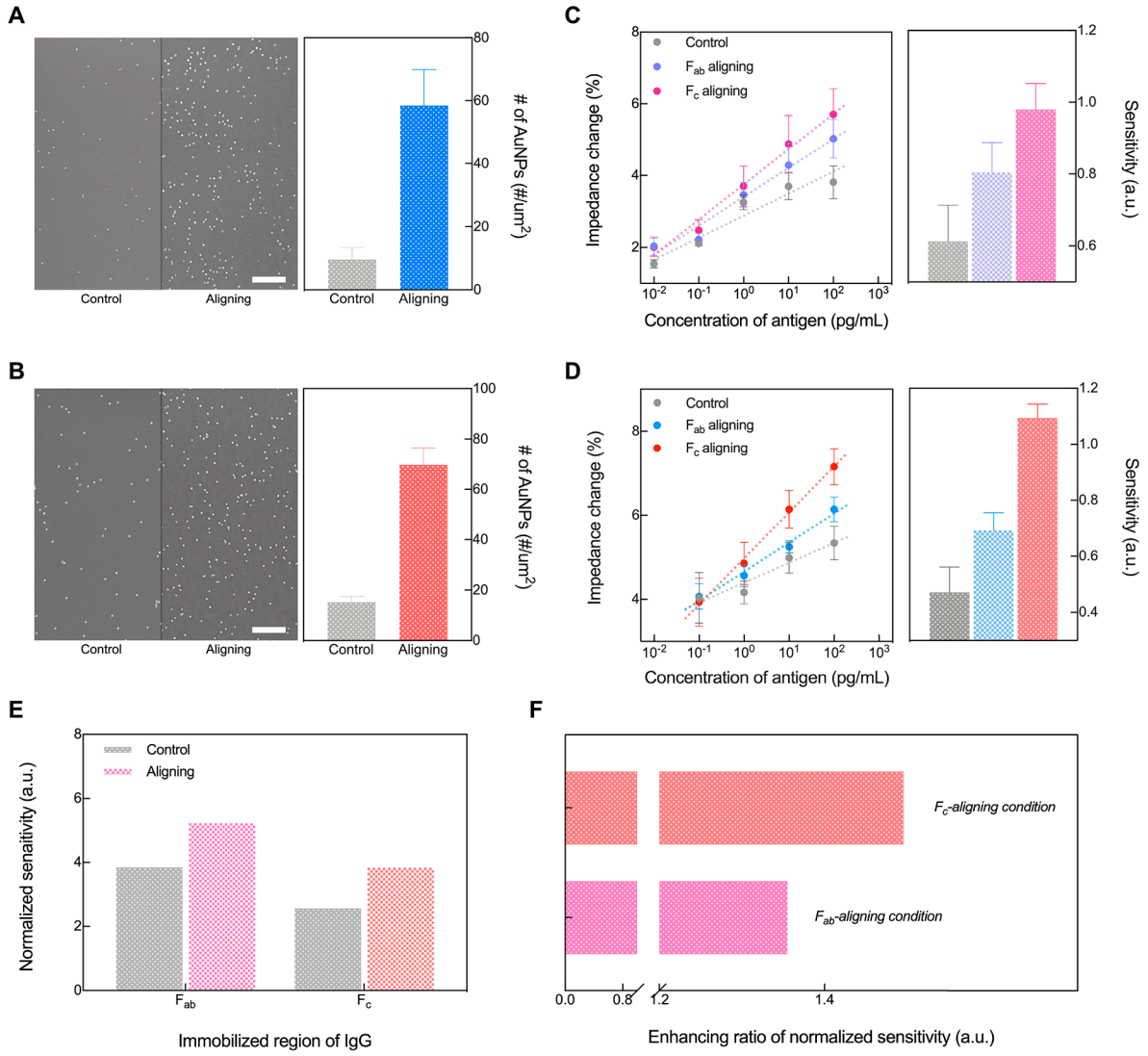

Figure 4. Binding efficiency enhancement between IgG and Aβ_{42} via IgG alignment. The number of AuNPs on the surface of sensor under the optimal (A) F_{ab}- and (B) F_c-aligning conditions. Scale bar = 0.5 μm. Enhanced sensitivity of the sensor measured in (C) PBS (10 mM) and (D) standard plasma. The gray scatters indicate the impedance values after Aβ_{42} binding to IgG under the control condition. (E) Normalized sensitivities under the control and the optimal IgG-aligning conditions. (F) Enhanced sensitivity per antibody immobilized density.

measured at any three random positions on the sensor surface (Figure S8). AuNP counts were ~9.57 ± 3.18 and ~58.4. ± 9.44 on the surface with immobilized F_{ab} under the control and the optimal F_{ab}-aligning condition, respectively (Figure 4A). Furthermore, the number of AuNP was ~15.23 ± 1.79 and ~69.67 ± 5.54 in the sensor in which the F_c region of IgG was immobilized under the control and optimal F_c-aligning condition, respectively (Figure 4B).

We also demonstrated the enhanced sensitivity of the sensor as a result of the IgG alignment by measuring the change in impedance following antigen binding at various concentrations in two types of buffers: PBS (10 mM) and standard plasma (1 mg mL^{-1}) both at pH 7.49. The antigen concentration in the buffer ranged from 10 fg mL^{-1} to 1 ng mL^{-1}. Under the control condition without aligning IgG, the changes in impedance measured in PBS ranged from ~1.54 ± 0.11% to ~4.03 ± 0.58%, and improved from ~2.03 ± 0.26% to ~5.19 ± 1.01% under the optimal F_{ab}-aligning condition (Figure 4C). These changes were further improved under the optimal F_c-aligning conditions from ~2.01 ± 0.26% to ~5.41 ± 0.55% according to antigen concentration. Given that the averaged noise level of the sensor was ~1.47 ± 0.10% (Figure S9), the dynamic range of the sensor was verified from 10 fg mL^{-1} to 100 pg mL^{-1}. The efficiency of IgG alignment was subsequently confirmed by comparing the enhanced sensitivity under each condition. The sensitivities calculated by linear regression analysis under the control and F_{ab}- and F_c-aligning conditions were ~0.61 ± 0.10, ~0.80 ± 0.08, and ~0.97 ± 0.07, respectively. Furthermore, the improved change in impedance due to the IgG aligning was demonstrated in the antigen detection in the standard plasma (Figure 4D). The changes in impedance under control conditions ranged from ~3.86 ± 0.40% to ~5.02 ± 0.35%, which were improved from ~3.98 ± 0.25% and ~6.56 ± 0.50% under the optimal F_{ab}- and F_c-aligning conditions, respectively. In addition, these changes improved from ~3.99 ± 0.60% to ~7.01 ± 0.74% under the optimal F_c-aligning condition. Accounting for noise, the dynamic range in plasma was confirmed at concentrations ranging from 100 fg mL^{-1} to 100 pg mL^{-1}, and the sensitivity in the dynamic range was ~0.47 ± 0.09, ~0.69 ± 0.06, and

https://doi.org/10.1021/acs.nanolett.2c01584
Nano Lett. 2022, 22, 6537−6544

~1.09 ± 0.05 under the control and the optimal F_{ab}- and F_c-aligning conditions, respectively. Consequently, the enhanced improvements in sensitivity resulting from aligning the F_{ab} and F_c regions were demonstrated to be ~1.31- and 1.60-fold in PBS, and ~1.41- and 2.18-fold in plasma, respectively.

Finally, we confirmed the normalized sensitivity obtained by diving the sensitivity values by each value of the aligned IgG density immobilized on the sensor surface. The normalized sensitivities were ~3.85 and ~2.56 in the control, and ~5.22 and ~3.84 in the F_{ab}- and F_c- aligning conditions, respectively (Figure 4E). Furthermore, the enhancing ratios of normalized sensitivities measured in the aligning condition compared with each value measured in the control condition were calculated to be 1.36 and 1.50 in the F_{ab}- and F_c-aligning conditions, respectively (Figure 4F). The results clearly demonstrate that the *E*-field mediated the alignment of IgG orientation, thereby enhancing the binding probability between IgG and antigen, which effectively improved the sensitivity of the biosensor.

CONCLUSION

Binding probability between the antibody and antigen is a crucial factor affecting the sensitivity and selectivity of biosensors. Our approach represents an improvement over the conventional methods, which are limited to chemical and biological IgG aligning, and is both cost-effective and convenient. The most commonly used methods to control the orientation of IgG include the use of a terminated or chemically functionalized self-assembled monolayer, IgG, and IgA. (Table S6).[41−43] Because these chemical/biological methods are likely to cause cross-reactions between substances when used simultaneously, sequential processing (long reaction time) and additional reagents (extra budget) are required to minimize the cross-reactions. On the other hand, aligning the IgG using *E*-fields can be easily integrated with chemical/biological aligning methods; hence, it is highly scalable when *E*-field sensors are used. For this reason, studies on IgG aligning using *E*-fields are currently underway; however, to the best of our knowledge, few studies have thus far confirmed the theoretical interpretation and experimental validation of aligning the IgG orientation based on *E*-field.

In this study, we confirmed that the binding probability between IgG and antigen increased as the orientation of IgG was controlled via the *E*-field. The single-step immobilization method is relatively simple but is limited in terms of controlling the orientation of the antibody. Although this can be compensated for through multistep immobilization methods based on chemical/biological linkers or heterogeneous functional supports, several limitations, such as material selection, time-consumption, and low controllability over the orientation of the antibody, remain to be addressed. Our multistep immobilization method using an *E*-field is efficient and can be universally used without restrictions on the antibody opening region on the substrate and materials since it is based on the dipole property, a general property of an antibody. Thus, our multistep immobilization method can be easily utilized for the realization of high-sensitivity biosensors capable of diagnosing various diseases, including AD. Although only IgG was used in the present study to validate the orientation alignment based on *E*-field, in the future, we plan to demonstrate the feasibility of our aligning method by specifically modeling the structures of various biomolecules, and applying highly sensitive biomolecule analysis.

ASSOCIATED CONTENT

Supporting Information

The Supporting Information is available free of charge at https://pubs.acs.org/doi/10.1021/acs.nanolett.2c01584.

Schematic diagram of the sensor surface on which the F_{ab} and F_c regions of IgG are immobilized, respectively; AFM images of the sensor surface; analysis of the AR of immobilized IgG in AFM images to confirm its orientation; AFM image of the sensor surface to which the antibody was not immobilized; ζ-potential of IgG based on the pH value of the buffer; changes in the impedance by immobilization of the F_{ab} and F_c regions of IgG in 10 mM PBS; alignment of the F_c region of IgA under various voltage conditions; scanning electron microscope (SEM) images under various immobilization conditions; noise level in the pure PBS and nonspecific signal level by adsorption of plasma protein under the optimal aligning conditions in the standard plasma; *E*-field intensity at the edge of the sensor electrodes; average ζ-potential values; changes in impedance caused by immobilized the F_{ab} region of IgG; changes in impedance caused by immobilized the F_c region of IgG; changes in impedance caused by antigen binding to the F_{ab} region of immobilized IgG; changes in impedance caused by antigen binding to the F_c region of immobilized IgG; summary of methods for aligning the IgG orientation; and simulation parameters (PDF)

AUTHOR INFORMATION

Corresponding Author

Jinsik Kim − *Department of Medical Biotechnology, College of Life Science and Biotechnology, Dongguk University, Seoul 04620, Republic of Korea;* orcid.org/0000-0002-9121-7031; Phone: +82-31-961-5155; Email: lookup2@dgu.ac.kr

Authors

Hye Jin Kim − *Center for Nanoparticle Research, Institute for Basic Science (IBS), Seoul 08826, Republic of Korea; Institute of Chemical Processes (ICP), Seoul National University, Seoul 08826, Republic of Korea*

Dongsung Park − *Department of Clinical Pharmacology and Therapeutics, College of Medicine, Kyung Hee University, Seoul 02447, Republic of Korea*

Yejin Park − *Department of Medical Biotechnology, College of Life Science and Biotechnology, Dongguk University, Seoul 04620, Republic of Korea*

Dae-Hyeong Kim − *Center for Nanoparticle Research, Institute for Basic Science (IBS), Seoul 08826, Republic of Korea; Department of Materials Science and Engineering, Seoul National University, Seoul 08826, Republic of Korea;* orcid.org/0000-0002-4722-1893

Complete contact information is available at: https://pubs.acs.org/10.1021/acs.nanolett.2c01584

Author Contributions

H.J.K. and J.K. conceived the idea of electric-field-mediated antibody alignment to enhance the antibody−antigen binding for ultrahigh sensitivity sensing. H.J.K. performed the simulation and most of the experiments. D.P. designed and performed the AFM analysis. Y.P. performed the antibody−antigen binding experiments. H.J.K., D.H.K., and J.K. wrote the

https://doi.org/10.1021/acs.nanolett.2c01584
Nano Lett. 2022, 22, 6537−6544

manuscript. D.H.K. and J.K. conceived and supervised the study. All authors reviewed and approved the manuscript.

Notes

The authors declare no competing financial interest.

■ ACKNOWLEDGMENTS

This work was financially supported by the National Research Foundation of Korea (NRF) funded by the Ministry of Education (NRF-2017R1C1B5075822, 2020R1F1A1076030, 2021R1C1C2004400), Korea Institute of Industrial Technology (KITECH, Republic of Korea, Project No. EO210011-02) and Technology Innovation Program (Project No. 20015793, funded by Ministry of Trade, Industry & Energy [MOITE, Korea]).

■ ABBREVIATIONS

Aβ_{42}, amyloid-beta 1−42; AD, Alzheimer's disease; AuNP, gold nanoparticle; *E*-field, electric-field; IgA, immunoglobulin A; IgG, immunoglobulin G; IMEs, interdigitated microelectrodes; PBS, phosphate-buffered saline; PI, isoelectric point

■ REFERENCES

(1) Wang, L.; Wang, X.; Wu, Y.; Guo, M.; Gu, C.; Dai, C.; Kong, D.; Wang, Y.; Zhang, C.; Qu, D.; Fan, C.; Xie, Y.; Zhu, Z.; Liu, Y.; Wei, D. Rapid and ultrasensitive electromechanical detection of ions, biomolecules and SARS-CoV-2 RNA in unamplified samples. *Nat. Biomed. Eng.* **2022**, *6*, 276−285.

(2) Chaibun, T.; Puenpa, J.; Ngamdee, T.; Boonapatcharoen, N.; Athamanolap, P.; O'Mullane, A. P.; Vongpunsawad, S.; Poovorawan, Y.; Lee, S. Y.; Lertanantawong, B. Rapid electrochemical detection of coronavirus SARS-CoV-2. *Nat. Commun.* **2021**, *12*, 802.

(3) Altug, H.; Oh, S. H.; Maier, S. A.; Homola, J. Advances and applications of nanophotonic biosensors. *Nat. Nanotechnol.* **2022**, *17*, 5−16.

(4) Song, S.; Singh, A. K.; Kirby, B. J. Electrophoretic concentration of proteins at laser-patterned nanoporous membranes in microchips. *Anal. Chem.* **2004**, *76*, 4589−4592.

(5) Kim, H. J.; Park, D.; Baek, S. Y.; Yang, S. H.; Kim, Y.; Lim, S. M.; Kim, J.; Hwang, K. S. Highly sensitive micropatterned interdigitated electrodes for enhancing the concentration effect based on dielectrophoresis. *Biosens. Bioelectron.* **2019**, *128*, 166−175.

(6) Qi, H.; Hu, Z.; Yang, Z.; Zhang, J.; Wu, J. J.; Cheng, C.; Wang, C.; Zheng, L. Capacitive aptasensor coupled with microfluidic enrichment for real-time detection of trace SARS-CoV-2 nucleocapsid protein. *Anal. Chem.* **2022**, *94*, 2812−2819.

(7) Park, M. Orientation control of the molecular recognition layer for improved sensitivity: a review. *BioChip J.* **2019**, *13*, 82−94.

(8) Ruiz, G.; Tripathi, K.; Okyem, S.; Driskell, J. D. pH impacts the orientation of antibody adsorbed onto gold nanoparticles. *Bioconjugate Chem.* **2019**, *30*, 1182−1191.

(9) Taheri, R. A.; Rezayan, A. H.; Rahimi, F.; Mohammadnejad, J.; Kamali, M. Comparison of antibody immobilization strategies in detection of Vibrio cholerae by surface plasmon resonance. *Biointerphases* **2016**, *11*, No. 041006.

(10) Shen, M.; Rusling, J. F.; Dixit, C. K. Site-selective orientated immobilization of antibodies and conjugates for immunodiagnostics development. *Methods* **2017**, *116*, 95−111.

(11) Huang, Z.; Raghuwanshi, V. S.; Garnier, G. Functionality of immunoglobulin g and immunoglobulin m antibody physisorbed on cellulosic films. *Front. Bioeng. Biotechnol.* **2017**, *5*, 41.

(12) Alves, N. J.; Kiziltepe, T.; Bilgicer, B. Oriented surface immobilization of antibodies at the conserved nucleotide binding site for enhanced antigen detection. *Langmuir* **2012**, *28*, 9640−9648.

(13) Batalla, P.; Mateo, C.; Grazu, V.; Fernandez-Lafuente, R.; Guisan, J. M. Covalent immobilization of antibodies on finally inert support surfaces through their surface regions having the highest densities in carboxyl groups. *Process Biochem.* **2009**, *44*, 365−368.

(14) Batalla, P.; Fuentes, M.; Mateo, C.; Grazu, V.; Fernandez-Lafuente, R.; Guisan, J. M. Covalent Immobilization of antibodies on finally inert support surfaces through their surface regions having the highest densities in carboxyl groups. *Biomacromolecules* **2008**, *9*, 2230−2236.

(15) Wieland, F.; Bruch, R.; Bergmann, M.; Partel, S.; Urban, G. A.; Dincer, C. Enhanced protein immobilization on polymers—a plasma surface activation study. *Polymers* **2020**, *12*, 104.

(16) Wujcik, E. K.; Wei, H.; Zhang, X.; Guo, J.; Yan, X.; Sutrave, N.; Wei, S.; Guo, Z. Antibody nanosensors: a detailed review. *RSC Adv.* **2014**, *4*, 43725−43745.

(17) Zhu, X.; Xiong, S.; Zhang, J.; Zhang, X.; Tong, X.; Kong, S. Improving paper-based ELISA performance through covalent immobilization of antibodies. *Sens. Actuators B: Chem.* **2018**, *255*, 598−604.

(18) Tajima, N.; Takai, M.; Ishihara, K. Significance of antibody orientation unraveled: well-oriented antibodies recorded high binding affinity. *Anal. Chem.* **2011**, *83*, 1969−1976.

(19) Jung, Y.; Lee, J. M.; Kim, J. W.; Yoon, J.; Cho, H.; Chung, B. H. Photoactivable antibody binding protein: site-selective and covalent coupling of antibody. *Anal. Chem.* **2009**, *81*, 936−942.

(20) Li, H.; Yan, J.; Ou, W.; Liu, H.; Liu, S.; Wan, Y. Construction of a biotinylated cameloid-like antibody for lable-free detection of apolipoprotein B-100. *Biosens. Bioelectron.* **2015**, *64*, 111−118.

(21) Khairil Anuar, N. A.; Banerjee, A.; Keeble, A. H.; Carella, A.; Nikov, G. I.; Howarth, M. Spy&Go purification of SpyTag-proteins using pseudo-SpyCatcher to access an oligomerization toolbox. *Nat. Commun.* **2019**, *10*, 1734.

(22) Guo, K.; Wustoni, S.; Koklu, A.; Díaz-Galicia, E.; Moser, M.; Hama, A.; Alqahtani, A. A.; Ahmad, A. N.; Alhamlan, F. S.; Shuaib, M.; Pain, A.; McCulloch, I.; Arold, S. T.; Grünberg, R.; Inal, S. Rapid single-molecule detection of COVID-19 and MERS antigens via nanobody-functionalized organic electrochemical transistors. *Nat. Biomed. Eng.* **2021**, *5*, 666−677.

(23) Gloag, L.; Mehdipour, M.; Chen, D.; Tilley, R. D.; Gooding, J. J. Advances in the application of magnetic nanoparticles for sensing. *Adv. Mater.* **2019**, *31*, 1904385.

(24) Gao, S.; Guisán, J. M.; Rocha-Martin, J. Oriented immobilization of antibodies onto sensing platforms- A critical review. *Anal. Chim. Acta* **2022**, *1189*, 338907.

(25) Chen, S.; Li, L.; Zhao, C.; Zheng, J. Surface hydration: Principles and applications toward low-fouling/nonfouling biomaterials. *Polymers* **2010**, *51*, 5283−5293.

(26) Walsh, S. J.; Bargh, J. D.; Dannheim, F. M.; Hanby, A. R.; Seki, H.; Counsell, A. J.; Ou, X.; Fowler, E.; Ashman, N.; Takada, Y.; Isidro-Llobet, A.; Parker, J. S.; Carroll, J. S.; Spring, D. R. Site-selective modification strategies in antibody−drug conjugates. *Chem. Soc. Rev.* **2021**, *50*, 1305−1353.

(27) Mullard, A. Synthetic lethality screens point the way to new cancer drug targets. *Nat. Rev. Drug Discovery* **2017**, *16*, 3−6.

(28) Lei, P.; Ayton, S.; Bush, A. The essential elements of Alzheimer's disease. *J. Biol. Chem.* **2021**, *296*, 100105.

(29) Davies, D. R.; Chacko, S. Antibody structure. *Acc. Chem. Res.* **1993**, *26*, 421−427.

(30) Edelman, G. M. Antibody structure and molecular immunology. *Science* **1973**, *180*, 830−840.

(31) Lou, D. D.; Ji, L.; Fan, L.; Ji, Y. X.; Gu, N.; Zhang, Y. Antibody-oriented strategy and mechanism for the preparation of fluorescent nanoprobes for fast and sensitive immunodetection. *Langmuir* **2019**, *35*, 4860−4867.

(32) Boswell, C. A.; Tesar, D. B.; Mukhyala, K.; Theil, F.-P.; Fielder, P. J.; Khawli, L. A. Effects of charge on antibody tissue distribution and pharmacokinetics. *Bioconjugate Chem.* **2010**, *21*, 2153−2163.

(33) Hebditch, M.; Warwicker, R. J. Web-based display of protein surface and pH-dependent properties for assessing the developability of biotherapeutics. *Sci. Rep.* **2019**, *9*, 1969.

https://doi.org/10.1021/acs.nanolett.2c01584
Nano Lett. 2022, 22, 6537−6544

(34) Shinoda, T.; Takahashi, N.; Takayasu, T.; Okuyama, T.; Shimizu, A. Complete amino acid sequence of the Fc region of a human delta chain. *Proc. Natl. Acad. Sci. U. S. A.* **1981**, *78*, 785−789.
(35) Polk, B. J.; Stelzenmuller, A.; Mijares, G.; MacCrehan, W.; Gaitan, M. Ag/AgCl microelectrodes with improved stability for microfluidics. *Sensor Actuat. B-Chem.* **2006**, *114*, 239−247.
(36) Zhou, J.; Tsao, H.-K.; Sheng, Y.-J; Jiang, S. Monte Carlo simulations of antibody adsorption and orientation on charged surfaces. *J. Chem. Phys.* **2004**, *121*, 1050−1057.
(37) Chen, S.; Liu, L.; Zhou, J.; Jiang, S. Controlling antibody orientation on charged self-assembled monolayers. *Langmuir* **2003**, *19*, 2859−2864.
(38) Emaminejad, S.; Javanmard, M.; Gupta, C.; Chang, S.; Davis, R. W.; Howe, R. T. Tunable control of antibody immobilization using electric field. *Proc. Natl. Acad. Sci. U. S. A.* **2015**, *112*, 1995−1999.
(39) Ghisellini, P.; Caiazzo, M.; Alessandrini, A.; Eggenhöffner, R.; Vassalli, M.; Facci, P. Direct electrical control of IgG conformation and functional activity at surfaces. *Sci. Rep.* **2016**, *6*, 37779.
(40) Bekard, I.; Dunstan, D. E. Electric field induced changes in protein conformation. *Soft Matter* **2014**, *10*, 431−437.
(41) Gajos, K.; Szafraniec, K.; Petrou, P.; Budkowski, A. Surface density dependent orientation and immunological recognition of antibody on silicon: TOF-SIMS and surface analysis of two covalent immobilization methods. *Appl. Surf. Sci.* **2020**, *518*, 146269.
(42) Seymour, E.; Unlu, N. L.; Carter, E. P.; Connor, J. H.; Unlu, M. S. Configurable digital virus counter on robust universal DNA chips. *ACS Sens.* **2021**, *6*, 229−237.
(43) Martin, L. J.; Akhavan, B.; Bilek, M. M. Electric fields control the orientation of peptides irreversibly immobilized on radical-functionalized surfaces. *Nat. Commun.* **2018**, *9*, 357.

https://doi.org/10.1021/acs.nanolett.2c01584
Nano Lett. 2022, 22, 6537−6544